Dynamic microstructure evolution in cold sprayed Ni-Ti composite coatings

Roghayeh Nikbakht [a]*, Mohammad Saadati [b], Hamid Assadi [c], Kamal Jahani [d], Bertrand Jodoin [a]

[a] Mechanical Engineering Department, University of Ottawa, 770 King Edward, Ottawa, Ontario, Canada

[b] Department of Mechanical Engineering, École de Technologie Supérieure (ETS), Montreal, QC, Canada

[c] Brunel Centre for Advanced Solidification Technology (BCAST), Brunel University London, Uxbridge, United Kingdom

[d] Mechanical Engineering Department, 29 Bahman Boulevard, University of Tabriz, Tabriz, Iran

Abstract

The severe plastic deformation inherent to cold spray provides a unique opportunity to study dynamic microstructure evolution under extremely high strain rates, not achievable in conventional laboratory experiments. In this study, the correlation between dynamic deformation and microstructure evolution is investigated for a heterogeneous system, using cold spray of blended Ni-Ti powder mixtures. EBSD analyses of the Ni and Ti splats show different degrees of dynamic recrystallization (DRX) especially at splat boundaries, which are attributed to different materials properties and dissimilar materials interaction. A heterogeneous structure of Ni-Ti composite was achieved with Ni splat being embedded in an ultra-fine grain Ti matrix with an average grain size of 500 nm. Results show hierarchical structures including twins with a thickness of about 500 nm, micro-bands and low angle boundaries, which are associated with a grain subdivision mechanism through continues dynamic recrystallization (CDRX). The results also demonstrate a drastically different response of Ti and Ni to the same loading conditions, hence provide an insight to the role of intrinsic material properties in DRX at extremely high strain rates.

Keywords: Dynamic Microstructure Evolution, Cold Spray Additive Manufacturing, EBSD Analysis, Ni-Ti Composite, DRX and CDRX, Twin and Micro-bands

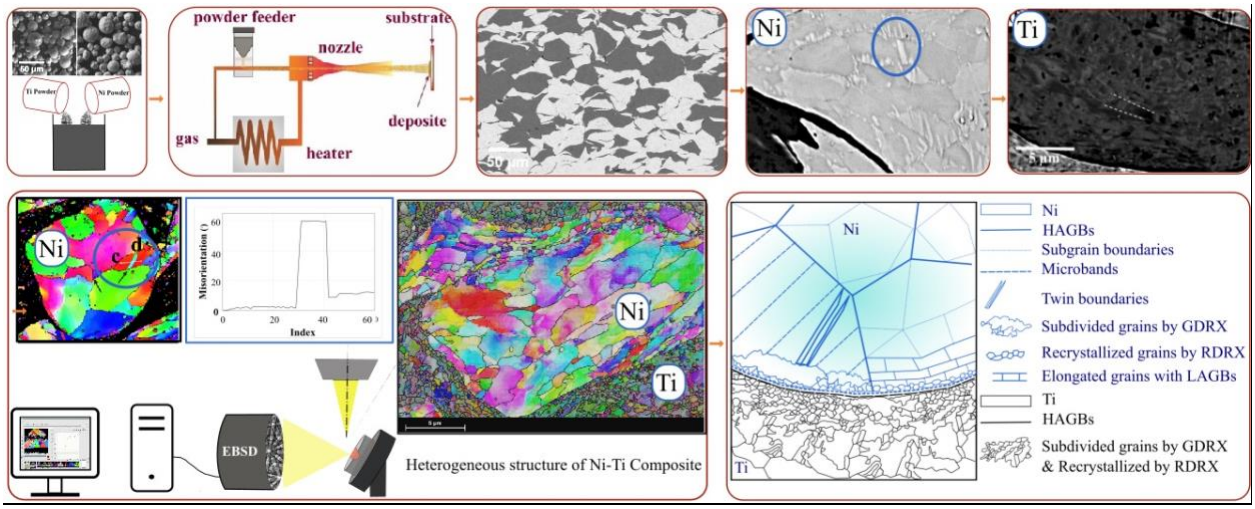

* Corresponding author. Tel. +16135625800, Ext:2481
E-mail address: roghayeh.nikbakht@uottawa.ca

1. Introduction

Over the past decades, significant improvement in material properties has been achieved with substantial grain refinement from micrometer to sub-micrometer or nanometer scale with various bottom-up or top-to-bottom technologies [1, 2]. Recently, heterogeneous and gradient structures have attracted a lot of attention because of their potential superior properties [3]. Different severe plastic deformation (SPD) based powder metallurgy processes involving SPD at the powder surface, through ball milling, high-pressure gas milling, etc., followed by sintering were used to manufacture harmonic structured materials [4].

Cold spray (CS) is a solid-state and high strain-rate powder consolidation method that can promote nanostructure and heterogeneous structure via severe plastic deformation while consolidating the powders in situ [5, 6]. CS is considered an additive manufacturing method in which particles are accelerated to high impact velocities (300-1200 m/s). Accelerated particles deposit on a substrate as a result of solid-state deformation at relatively low temperatures and at velocities around or beyond a material-dependent critical velocity at which the bonding strength of particles overcomes their rebounding elastic forces [7-9]. Therefore, each individual particle experiences severe plastic deformation, specifically at particle boundaries. The high strain rate and successive impact of particles promote heterogeneous dynamic microstructure evolution in coating microstructure. Process parameters, including inlet gas pressure and temperature, dictate the particle deformation and heterogeneous microstructure evolution by controlling particle temperature and velocity. Zener-Hollomon-based analysis has been used to explore the effect of process parameters in heterogeneous microstructure evolution of copper coating upon CS deposition [6]. EBSD analysis of Al-2Cu and Al-5Cu single particles upon high-velocity impact showed that ultrafine grains formed at the particle/particle interface, and an amorphous layer was observed at Al-Cu

(particle)/Steel (substrate) interface [10]. Microstructure studies of CS single-particle Ti showed that fine equiaxed grains from at splat boundaries with some elongated grains in the inner boundary of Ti splat [11]. The equiaxed, fine grains are believed to be formed by the non-diffusional recrystallization mechanism [10-12].

In addition to microstructure heterogeneity of individual materials inherent to CS (from splat boundaries to the center of the splat) dictated by process parameters, different deformation behavior and microstructure heterogeneity were reported in CS of mixed powders as a result of different material properties of each component [13]. Furthermore, bonding analysis of mismatch materials showed that dissimilar materials have different critical velocities than similar impact. Therefore, it remains an open question if dissimilar impact in composite coatings can change the dynamic microstructure evolution of materials than their single-component coating in a similar process condition. In this work, a Ni-Ti composite has been considered a model material system to explore the heterogeneous microstructure evolution of CS composite materials.

The selection of the Ni-Ti system for the CS process in the current study is based on the fact that pure Ni and pure Ti with FCC and HCP crystal structures and dissimilar thermal and mechanical properties have different deformation behavior during CS . Under the high strain rate experienced by metals during CS, the main obstacles to dislocation glide are lattice friction and the dislocation interactions with the dislocations network and grain boundaries [14, 15]. Friction stress (Peierls term) is a function of strain rate and temperature. It includes a significant portion of the flow stress of HCP metals and alloys at low temperatures and high strain rates, whereas its contribution to the flow stress of FCC metals and alloys is negligibly small [15]. Therefore, it is expected that these two materials experience different deformation behavior upon high strain rate deformation, which potentially can result in different grain refinement and heterogeneity. The objective of this work

is to explore the deformation microstructure and grain refinement evolution of CS Ni-Ti components. Finite element modeling (FEM) has been used to explore the effect of deformation field variables, including stress, strain, strain rate, and temperature, on dynamic microstructure evolution.

2. Experimental procedure

The composite Ni-Ti coating was sprayed using spherical gas atomized Ni powder (CP-Ni, Atlantic Equipment Engineers, Upper Saddle River, NJ, USA) and Ti powder (CP-Ti Grade 1, Advanced Powder and Coatings, Boisbriand, Canada) with the mean particle sizes of 24.5 μm and 30.7 μm, respectively. The feedstock powder mixed with the composition of 79Ni-21Ti wt.% was sprayed using the EP Series SST Cold Spray System (Centerline (Windsor) Ltd., Canada) with stainless steel nozzle and Nitrogen as a propellant gas at gas temperature and pressure of 500 ˚C and 3.4 MPa [16, 17].

The microstructures of the coatings were analyzed using scanning electron microscopy (SEM) (EVO MA-10, Carl Zeiss AG, Oberkochen, Germany) and electron backscattered diffraction (EBSD) analyses using a SU-8230 Hitachi cold field emission SEM equipped with a Bruker e^- Flash HR^+ EBSD detector. This work approached EBSD indexation enhancement of a highly deformed microstructure of deposited Ni-Ti composites through different preparation methods and low-temperature annealing. Using a combination of Vibromet polishing and Ar ion milling, the Ni phase of the composite Ni-Ti sample was indexed when the Ti phase had a lower confidence index. Annealing treatment at 290 ˚C was used to enhance the indexation quality, specifically for the Ti phase, where other surface preparation did not lead to satisfactory results [18]. The annealing

temperature was low enough (290˚C, lower than the homologous recrystallization temperature (HRT) of Ni and specifically Ti) to make sure that static recrystallization (SRX) would not change the microstructure evolution from as-sprayed microstructure.

3. FEM Modelling

Axisymmetric FEM models were employed using the commercially available finite element software ABAQUS to gain more insight into deformation field variable evolution upon high strain rate deformation of the composite coating. The mesh size of both the substrate and the particles near the contact surface was set to be a maximum of 1/50 of the particle diameter. Distortion control values were used to alleviate severe distortion of the elements due to high-velocity impact. The mean particle size of 25 μm was used for simulation. The measured particle velocity for Ni was respectively 456 ± 70. Therefore, the initial particle velocity was set to 500 m/s in the model for Ni (particle)/Ti (substrate). The general physical properties of powders and substrate materials used in the models are given in Table 1. The initial substrate and particle temperature were set to 298 K.

The material state in the high-pressure domain and shock wave propagation condition was defined by the ‘‘Mie- Grüneisen’’ equation of state (EOS) and was used in the linear Hugoniot formulation [17]:

$$p = \frac{\rho_0 c_0^2 \eta}{(1 - s\eta)^2}\left(1 - \frac{\Gamma_0 \eta}{2}\right) + \Gamma_0 \rho_0 E_m \qquad (1)$$

$$\eta = 1 - \frac{\rho_0}{\rho} \tag{2}$$

where p is the hydrodynamic stress, ρ_0 is the initial density, c_0 is the material speed of sound, s is the Hugoniot slope coefficient, Γ_0 is the Grüneisen constant, E_m is the internal energy per unit mass, and ρ is the density.

The deviatoric stress of elastic response was assumed to be linear :

$$d = 2G_e\varepsilon_s \tag{3}$$

where d is the deviatoric stress G_e is the elastic shear modulus and ε_s is the elastic deviatoric strain. The EOS parameters of the powders and substrate materials used in the simulations were presented in Table 1 [17].

Table 1. FEM Modelling parameters

Property	Symbol	unit	Ni	Ti
Conductivity	k	W/(m K)	91	11.4
Density	ρ	kg/m^3	8890	4510
Elastic Shear Modulus	G	GPa	76	30
Speed of sound	C_0	m/s	4542	5020
Gruüneisen's constant	Γ_0	-	1.83	1.23
Hugoniot slope	s	-	1.5	1.53
Specific heat	C_p	J/(kg /K)	456	528
Melting Temp	T_m	K	1726	1923
Jonson Cook	A	MPa	163	806.57
	B	MPa	648	481.61
	n	-	0.33	0.319
	C	-	0.006	0.0194
	m	-	1.44	0.655

The plastic behavior of impacting particles and substrates during dynamic deformation was described by the Johnson-Cook model (equation 4), and material parameters were presented in Table 1 [17, 19].

$$\sigma_{JC} = (A + B\varepsilon^{n})(1 + C\ln\frac{\dot{\varepsilon}}{\dot{\varepsilon}_0})[1 - (\frac{T - T_0}{T_m - T_0})^{m}] \quad (4)$$

The strain hardening, strain rate hardening and thermal softening were considered in this model .

4. Results and discussion

4.1. Deformation microstructure evolution

The cross-sections of the Ti and Ni powders are presented in Figs.1 (a) and (b), respectively. The etched cross-section of Ti particle illustrates an acicular α-Ti structure which is common in atomized pure titanium powders. Ni particle has fine micron-size equiaxed grains with a distribution between 1-5 μm. The cross-section image of the composite Ni-Ti sample is presented in Fig. 1(c). Both Ni and Ti splats of Fig 1 (c) (with light and dark gray contrast, respectively) are well deformed and coalesced in the microstructure. The EDS analysis of this sample (not presented here) showed that the composition of the coating is very close to equiatomic composition (49.4 at.% Ti and balanced Ni). The higher magnification image of the selected area of coating in Fig. 1(d) shows a Ni splat substructure. Some linear substructural features similar to either micro twinning or micro-bands can be seen inside the grains of as-sprayed Ni particles (marked with arrows in Fig. 1 (d)), while there is no sign of these features in the as-received Ni particles. It has been reported that high strain rate deformations at relatively low temperatures might introduce

deformation mechanism transition from dislocation glide and climb to deformation twinning in conventional high and medium stacking fault energy (SFE) metals such as Al (180 mJm^{-2}) and Ni (130 mJm^{-2}) similar to low SFE metals [20-22].

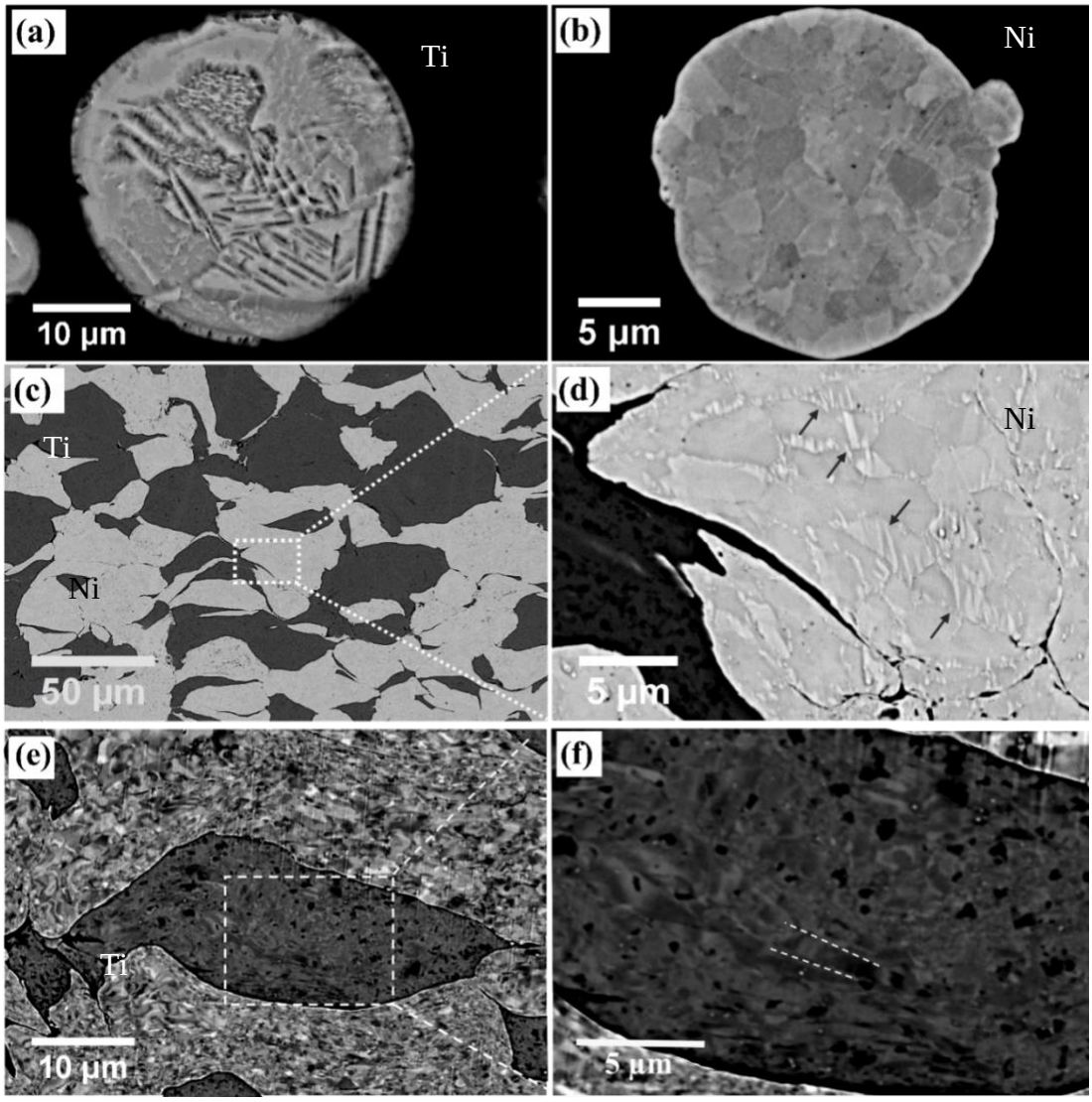

Figure 1. (a) Cross section of as-received Ti powder particle (etched) and (b) ECCI map of Ni powder particle cross section, (c) SEM image of Ni-Ti composite coating, (d) deformed Ni particle of the composite coating, (e-f) ECCI maps of coating cross section which shows Ti splat in Ni matrix.

Accordingly, micro twin formation in single splats of copper and copper coatings was reported [23-25]. Bae et al. [26] stated that nanoscale deformation twinnings formed in CS of nano-size grain Ni deposits parallel to the {111} planes near the oxides at the bonded interface of Ni splats. However, the microstructural features observed in the Ni splat of Fig. 1 (d) are neither limited to the Ni particle splat boundaries nor are nano-sized. They are rather microscale features observable inside the splat grains and at the splat grain boundaries, which first appeared near or at the Ni grain boundaries and propagated inside the grains. Taking into consideration that the impact direction of the coating is top to bottom (Fig. 1 (d)), one can imply that the linear features have a specific orientation with impact direction, which supports the notion that they have some relation with the loading direction, thereby they are deformation related features.

The electron channeling contrast imaging (ECCI) maps of the sample in Figs. 1 (e) and (f) illustrate the substructure of Ni and Ti splats after deformation. Comparison of deformed microstructure with as-received particle cross-sections demonstrates that both Ni and Ti underwent severe plastic deformation. A closer look at Ti splat (Fig. 1 (f)) shows refined grain structure at splat boundaries and some elongated and linear structure next to the refined structure toward the center of the splat. TEM and ECCI analysis of a single particle of Ti speculated that these elongated structures are either twins or elongated low angle boundaries [27], which did not succeed to recrystallize as the temperature inside the splats were not high enough [11, 27, 28].

Figures 2 (a-c) show band contrast (BC), inverse pole figure (IPF), and Kernel average misorientation (KAM) maps of the composite coating. Some linear structures can be seen inside the Ni splats (marked with circles in Fig. 2 (b)). Additionally, some linear orientation variation - with significant misorientations can be seen inside some grains (the grain outlined in the bottom of Figs. 2(b) and (c)).

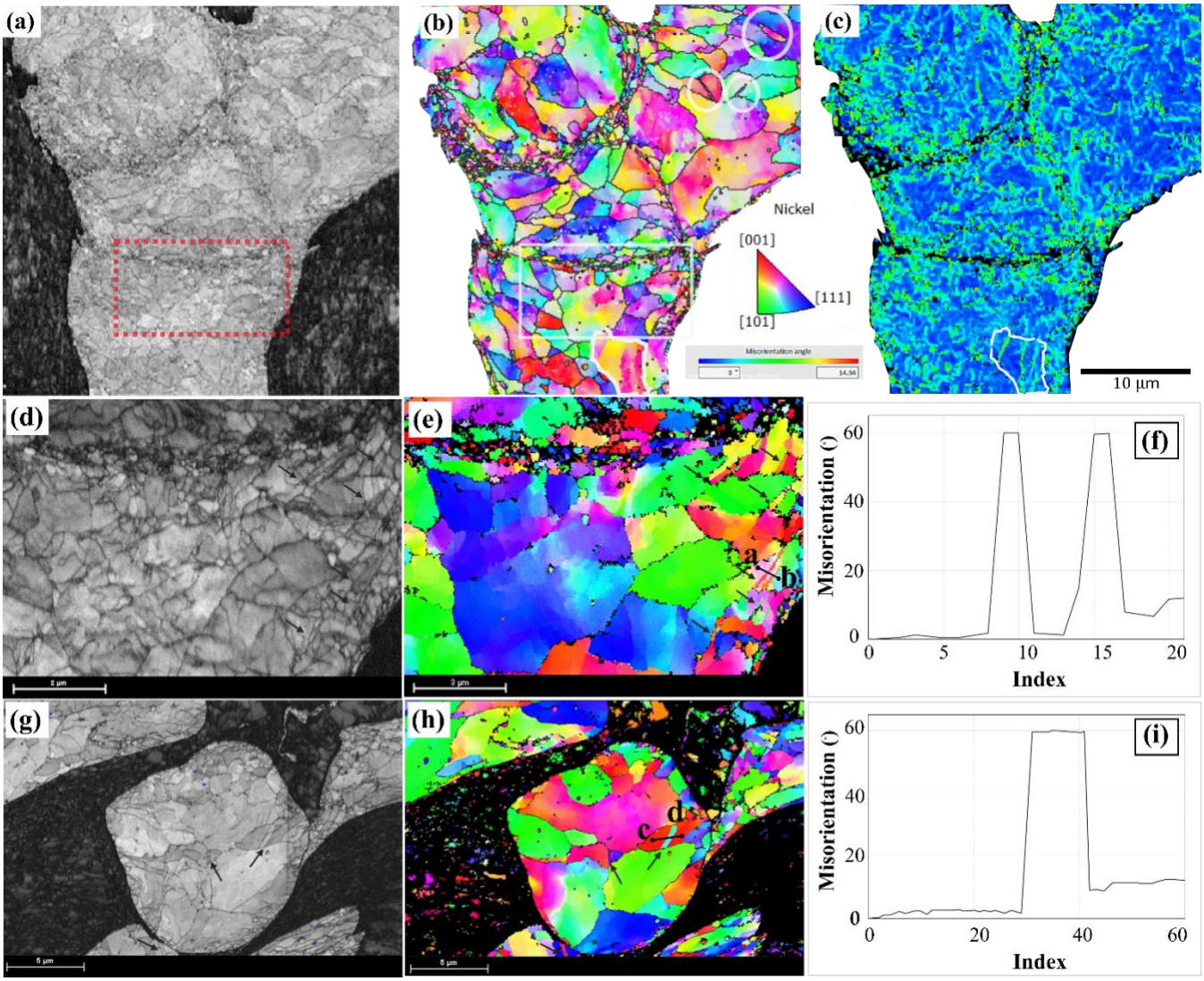

Figure 2. EBSD analysis of as-sprayed and annealed coating with impact direction from top to bottom. (a) BC map of the as-sprayed composite coating, (b) IPFZ of the microstructure of Ni splats with high angle grain boundary, (c) KAM map of Ni splat of Fig (a), (d) BC map of the selected area of Fig. (a) at higher magnification, (e) IPFX of the selected area of Fig. (b) at higher magnification, (f) misorientation analysis of the marked line in Fig. (e), (g) BC of annealed nickel splat in titanium matrix, (h) IPFZ of (g), and (i) misorientation analysis of the marked line in Fig. (g).

The higher magnification image of selected areas (Figs. 2 (d) and (e)) and annealed sample in Figs. 2(g) and (h)) demonstrate the similar linear features are observed at the grains of Ni splats (marked with arrows) close to impact boundaries. The linear features have a different orientation from parent grains. The point to origin orientation variations of some of these linear features in respect to parent grains are plotted in Figs. 2 (f) and (i) along the lines from a-b and c-d, respectively, in Figs. 2 (e) and (h). The analyzed linear features show ~60 degrees misorientation with the parent grain, which is the characteristic of {111}<112> deformation twinning in FCC metals [29]. Therefore, it can be concluded that deformation twins form at the interior and boundary grains' of Nickel splats.

For further investigation, boundaries with different misorientations were plotted on the BC map in Fig. 3. One can see from Figs. 3 (a) and (b) that some linear features are observed at the interior of the Ni splat, which has less misorientation with the parent grains. This means that high angle boundaries (HAGB) and low angle boundaries (LAGB) with linear substructures develop during high strain rate deformation of Ni. Most of the linear substructures, regardless of their misorientation, have almost similar inclination angles with impact direction, from top to bottom. Additionally, one can see that the HAGBs (linear and nonlinear) are more prevalent at splat boundaries.

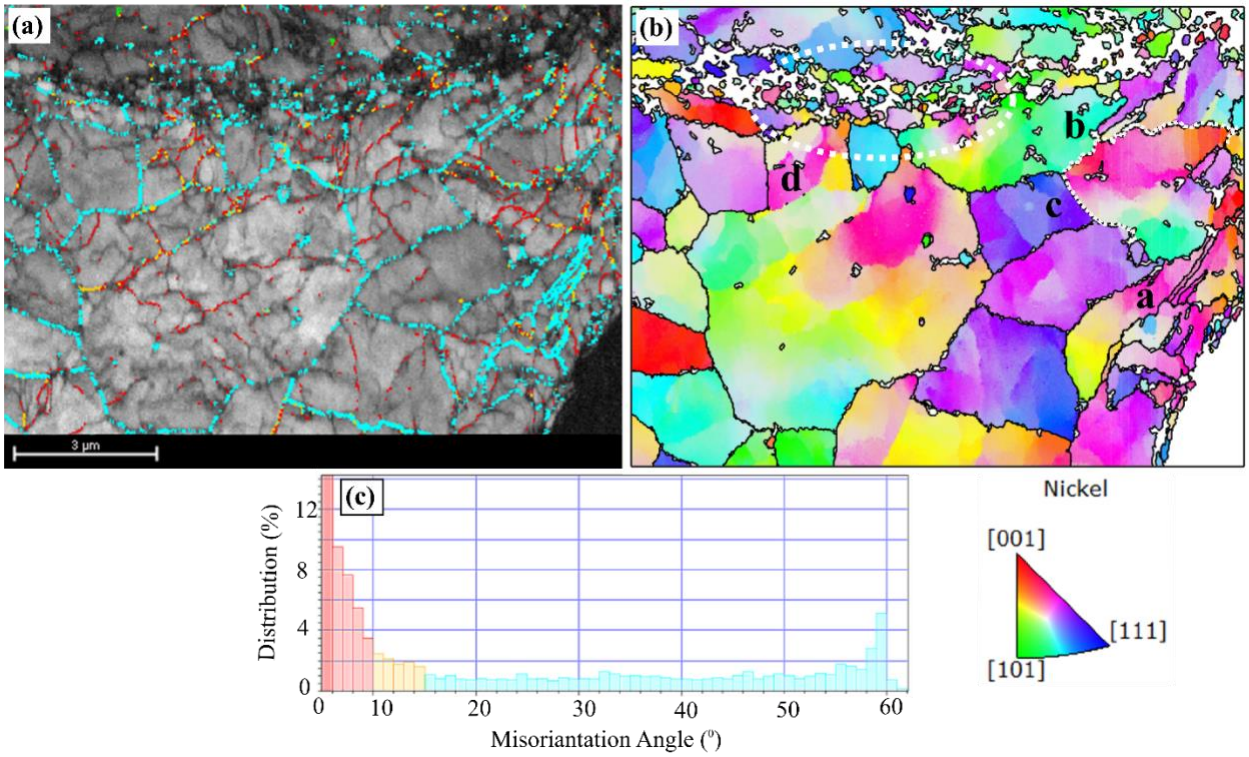

Figure 3. (a) BC map with boundaries misorientation of Ni splat of as-sprayed composite coating, (b) IPFZ and (c) misorientation distribution.

Figs. 4 (a-c) indicate BC map, IPF, and phase map of the composite coating. Two Ni splats can be seen inside the Ti matrix. Similar linear structures can be seen in Ni splat boundaries and the center of the upper splat (Fig. 4(b)), which experienced more deformation than the lower splat. Consequently, one can conclude that deformation micro twins form at Ni splats of composite Ni-Ti coating with a thickness of almost 0.5 µm as a result of high strain rate deformation (Fig. 2 (e) and (h)). Very fine nano twins with a thickness of 15 nm were reported in CS of Ni, which has been explained with the impurities effect on the decrease of SFE at splat boundaries [23, 26]. The Ni powder used in this work had a commercial purity of 99.9 wt.%, and the twins formed not only at splat boundaries but also at the interior of the splats.

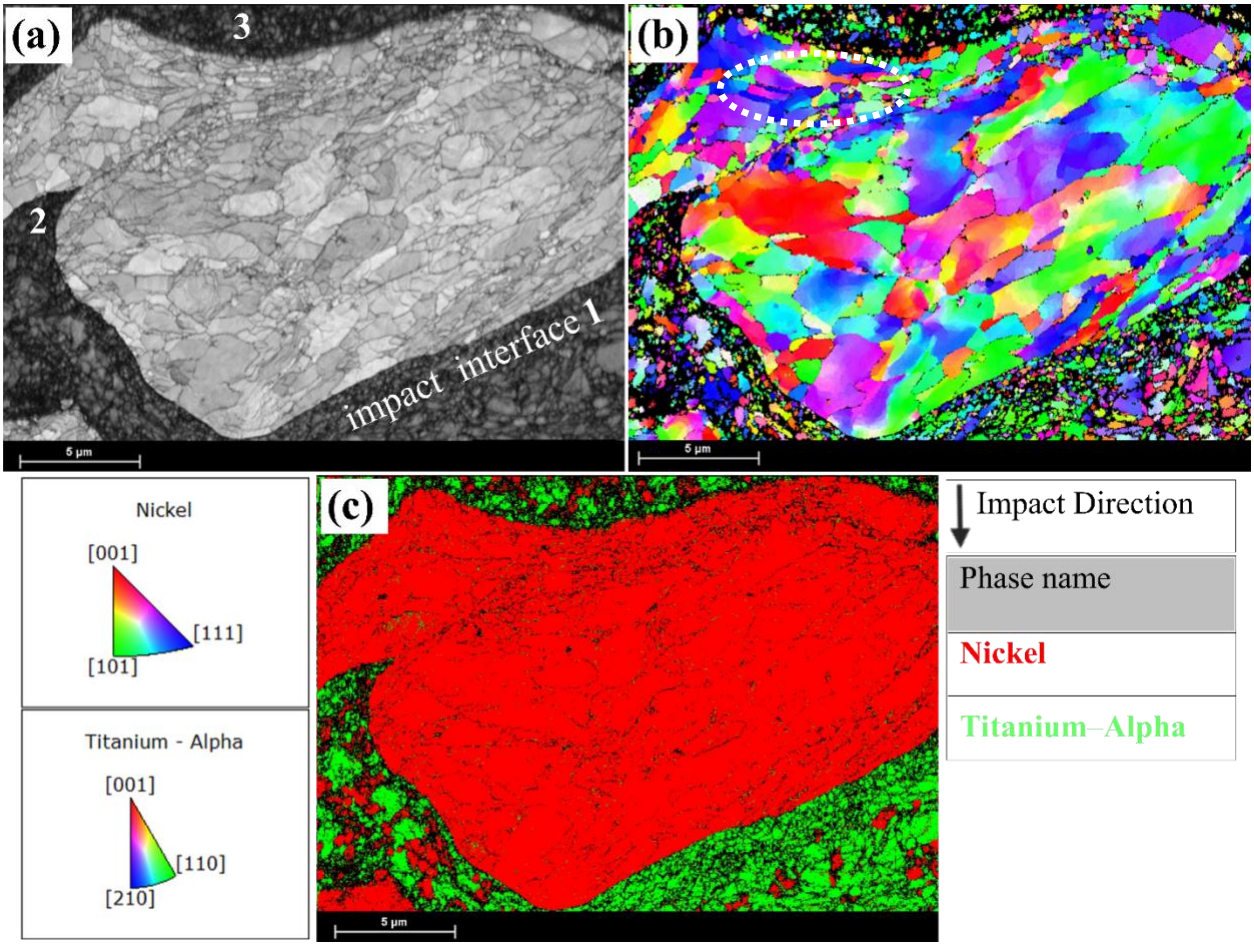

Figure 4. EBSD analysis of composite coating (annealed at 290 ℃). (a) BC map of the microstructure with Ni and Ti in light and dark contrast, (b) IPFZ image of the microstructure, (c) phase map, nickel and titanium are red and green, respectively.

The EBSD analysis proved that mechanical twins (with misorientation of about 60 degrees) form at the Ni splats. Regarding the linear structures with lower misorientation boundaries, one might argue that those elongated structures are LAGBs similar to sub-grain boundaries in the interior of original large grains. In this regard, the combined BC, IPFZ, and HAGBs mapped in Fig. 5 shows that the elongated structures might have different nature: The orientation variation can be seen at some elongated structures at the splat boundaries while the others have more linear boundaries

with no much orientation variation (a and b respectively in Fig. 5). However, the lamellar nature of these features combined with their preferential orientation rule out the hypothesis that they are simply LAGBs or sub-grain boundaries, specifically those with sharp linear interfaces (b and c in Fig. 3 (b) and b in Fig. 5). Putting all these points together, one can imply that some of these linear features, particularly those with less misorientation from parent grains (lower than 60 degrees), are micro-bands, specifically those far from the splat interface. This means that they experienced less deformation (strains) at lower strain rates and potentially have lower temperature rise as a result of adiabatic heating during deformation. Fig. 3 (a) shows some linear features with a combination of low and high misorientation angle (b in Fig. 3 (b)) and low misorientation (c in Fig. 3 (b)), which can be considered as deformation twins in a, combination of twinning and micro-bands in b, and micro-bands in c, which was also reported in shock loading of nickel [30]. Although particle impact velocity in CS is relatively lower than shock loading experiments, the simulation showed that local pressure at the interface of the multi-particle impact of Ni could reach values as high as 25 GPa. The pressure of slip to twinning transition is a function of particle size and decreases with the increase of particle size in such a way that this pressure for pure Ni is in the range of 25 to 36 GPa for grain distribution of 5 to 1 μm, respectively.

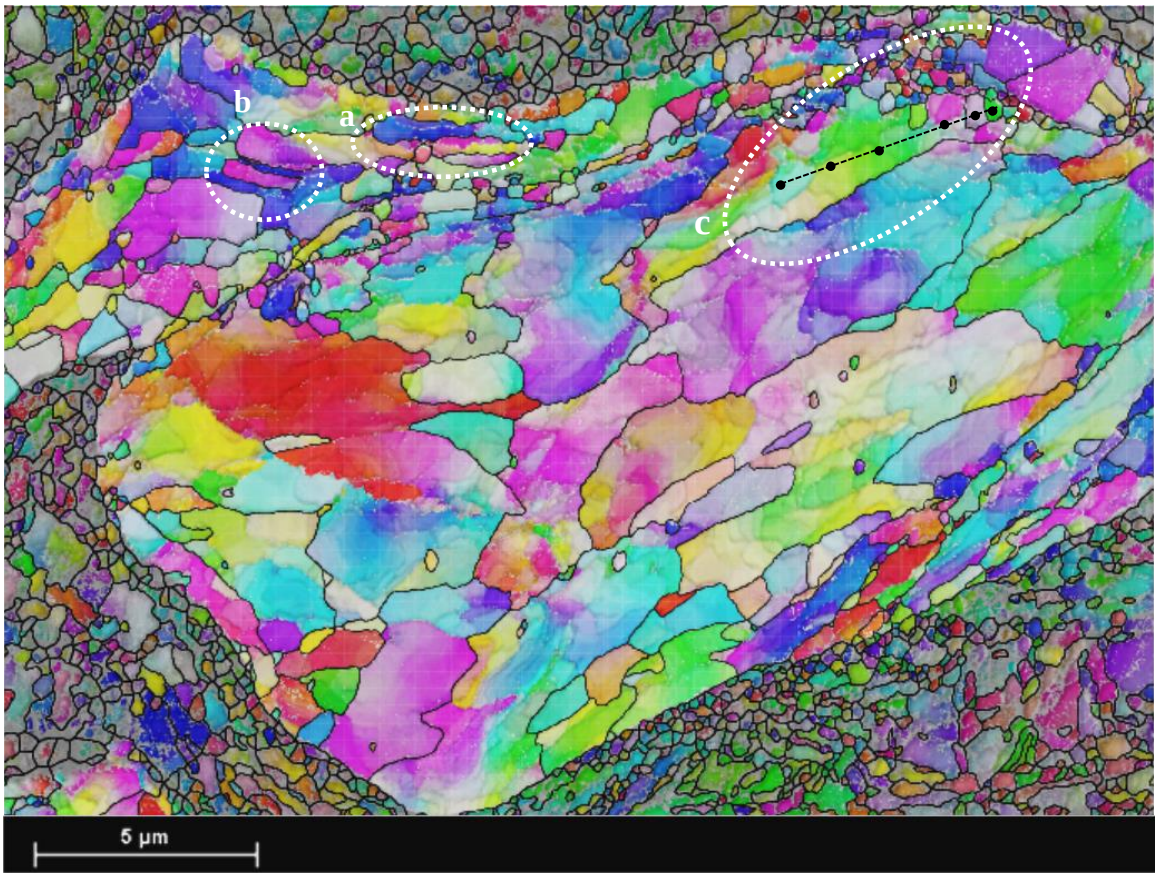

Figure 5. Hierarchical and heterogeneous microstructure of cold sprayed composite Ni-Ti coating. Combined BC and IPFZ map of the composite coating. Grain boundaries with misorientation of higher than 15 degrees have been shown on the map.

The distributions of deformation field variables were extracted from FEM simulation of Ni particle impact and presented in Fig. 6. The Tresca stress is considered here to show equivalent shear stress distribution. In a simple definition, this criterion is equivalent to a critical value of the maximum shear stress of yielding, which involves slip and dislocation motion. Strain rate, strain, and temperature are other field variables that affect the deformation microstructure evolution. Tresca shear stress and strain rate distribution (Fig. 6 (a)) extended from the splat boundary toward the center of the splat, and both have their maximum values (1.23 GPA and $1.15\times10^{8}\ S^{-1}$, respectively) at the sheared zone of the splat boundary. Temperature and equivalent plastic strain (PEEQ)

distributions in Fig. 6 (b) show that impacted particles experience the highest temperature increase and PEEQ at the sheared zone of the splat [31]. The presented field variables distributions show that individual particle experiences severe plastic deformation with a gradient in strain, strain rate, and temperature from particle boundaries toward the particle interior.

Moreover, the simulation results show that the deformation time scale of CS particles is on the order of the nanoseconds with high shear stress at splat boundaries - reaching values as high as 1.23 GPa at splat boundaries- while dislocations propagate in solids at the scale of the speed of sound. Therefore, based on strain and strain rate level, deformation can be accommodated either by formation of twinning at highly strained impact interfaces or by micro-bands. In terms of twinning, it happens when the slip system is restricted, or the critical shear stress of twinning is reached (low temperature or high strain rate deformation).

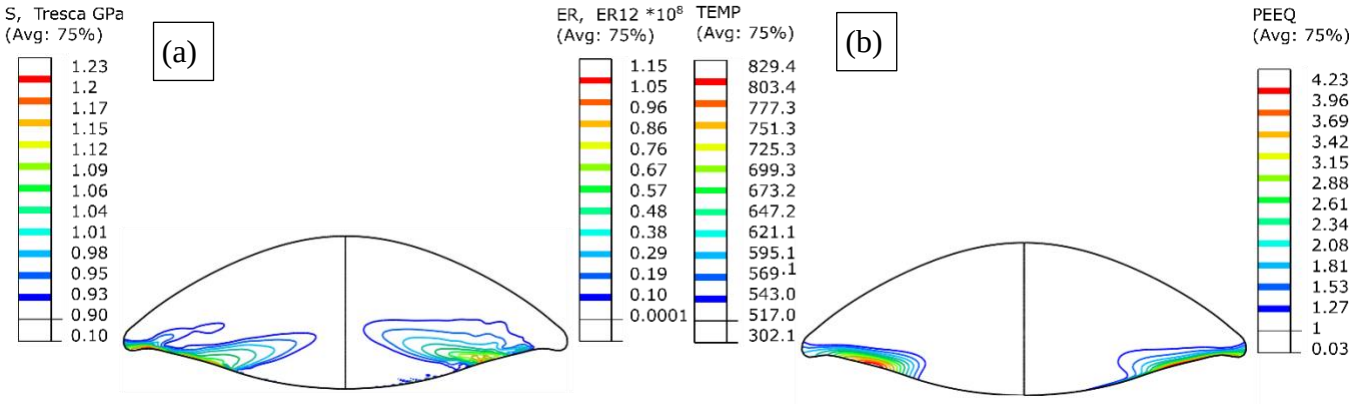

Figure 6. FEM modelling of Ni particle at an impact velocity of 500 m/s. (a) Distribution of the Tresca stress and shear strain rate distribution (ER12) at 36 ns after impact are presented in the left and right half of the particle, (b) temperature and equivalent plastic strain (PEEQ) distribution of splat in left and right of the splat. Temperature and PEEQ distributions were drawn respectively for values above 517 K (0.3 T_m Nickel) and 1.

For the shear stresses lower than the critical shear stress of twinning, planar glide of dislocations (as a consequence of high strain rate deformation) results in micro-bands formation as dislocations do not have enough time to move out of slip plans and aggregates on {111} slip planes (in FCCs) as crystallographic or non-crystallographic micro-bands based on strain and strain rate level. Micro-bands (or deformation bands) might form when individual grains within the splat subdivide extensively into regions of different orientations during deformation due to inhomogeneous stresses transmitted by neighboring grains [32]. The resulting deformation bands deform on different slip systems and may develop widely divergent orientations. Twinning, and micro-bands with the creation of new boundaries, can be considered as one of the grain subdivision mechanisms in CS Ni, giving rise to a hierarchical distribution of grains.

4.2.Heterogeneous microstructure evolution mechanism

The overall deformation appears to be inhomogeneous, with elongated and equiaxed grains co-existing at both Ni and Ti splats. A close look at the Ni splat boundaries from Figs. 2-5 shows that different degrees of dynamic recrystallization (DRX) took place at the highly strained areas of the splat boundaries (Fig. 6). The Ni splats in Figs. 4 and 5 show a bimodal heterogeneous microstructure with fine substructure at impact boundaries and large grains at the interior of the Ni splat, which is not significantly different from as-sprayed samples in terms of microstructure characteristics and grain distribution (Figs. 2-3) proving the fact that the annealing mostly improved indexation with an insignificant change of the microstructure. Fine necklace like grains formed at splat boundaries as a result of DRX, while large grains are seen inside the splats. In some interface areas, only elongated LAGBs can be seen (a in Fig. 5). Moreover, one can see from Fig. 3 (a) that the misorientation of the boundaries decreases from splat boundaries to splat interior

as a result of the gradual decrease in deformation field variables, including stress, strain, strain rate, and temperature. Deformation is accommodated more by dislocation cell and sub-grain formation, though very few fine recrystallized grains formed close to grain boundaries of the original large grains at the splat interior. Considering the spray conditions and modeling results (Fig. 6), one can see that the central part of the particles remains at temperatures lower than the HRT of Ti and Ni [17]. This assumption rules out the role of static recovery (SRV) or static recrystallization (SRX) in the central part of the splats and supports the role of dynamic recovery (DRV) and DRX. At Ni splat boundaries, HAGBs are more prevailing, which are either fine dynamically recrystallized grains or twin boundaries-divided grains. This eventually gives rise to a distinctly inhomogeneous grain microstructure comprising a mixture of relatively coarse non-refined original grains, grains with sub-grains or LAGBs, and fine recrystallized grains.

Ti splats interface areas are largely recrystallized and form very fine grains (<1.4 μm) with an average grain size of 0.52 μm. Ni splats have bimodal grain distribution, including fine refined grain with an average grain size of about 1.5 μm and large grains with an overall average grain size of 5.1 μm. The larger grains seem to have preserved the mean grain size of about 5 μm, which was originally present in the feedstock powder particles with some orientation variation and sub-grain boundaries formed inside these grains. The grain refinement is more conspicuous for Ti in all interface areas (both Ni/Ti and Ti/Ni interfaces), while for Ni splat, fine grains are more likely at Ni/Ni interface. Figure 5 clearly shows the Ni splats in a fine matrix of Ti grains. These differences in the deformation and grain refinement's prevalence can be related to lower shear localization strain of Ti stemming from its low heat conductivity and strain hardening rate and high adiabatic shearing sensitivity (softening) compared to Ni, which results in more prevailing shear banding and DRX.

Single-particle of Ti at impact velocities of 724 m/s showed some lamellar structure formed with a limited refined area close to impact interface, while fine recrystallized grains with good bonding were achieved at an impact velocity of 825 m/s with substrate preheating [28]. The Ti splats in Ni-Ti coatings, on the other hand, were flattened, well deformed, and recrystallized as a result of the tamping effect of high-density Ni at an average impact velocity of 500 m/s and particle temperature close to room temperature. This suggests that the deformation and grain refinement mechanisms of Ti is different from those of single-component powder. The composition of mixed powders was 24.6 at.% Ti and 76.4 at.% Ni, while an equiatomic composition was achieved for the deposited coating, which meant that the relative deposition efficiency (DE) of Ni was almost three times lower than Ti [33]. The lower DE of Ni contributed to splat deformation (specifically Ti splats deformation) with a hammering effect. This implies that the interaction among dissimilar materials can significantly change the dynamic microstructure evolution of individual materials in composite coating compared to their single-component coatings even when the process parameter (including velocity, temperature) are fixed. This is one of the aspects of heterogeneity of microstructure, which is achieved as a result of different deformation and recrystallization behavior of the components in CS of composite coatings. Such splat-boundary grain refinement results in gradient structure upon intermetallics evolution in post-spay heat treatment of Ni-Ti [16].

The schematic of microstructure evolution of Ni and Ti at Ni/Ti interface is shown in Fig. 7. The schematic summarizes the observed results and reported grain refinement mechanisms of Ni and Ti. The fast deformation of particles in CS (in the order of nanoseconds) inhibits diffusion-based grain-boundary migrations, which rules out the migrational recrystallization contribution in dynamic recrystallization [12, 34]. Considering the downstream feeding of the powder particles (using a low-pressure CS system) with not very high inlet gas temperature (500 ˚C), the particles

upon deposition are cold enough to rule out the role of SRX and SRV in the microstructure evolution of Ni-Ti coating in general. Therefore, continuous dynamic recrystallization (CDRX), which is phenomenologically attributed to any DRX other than nucleation and growth mechanism, is considered the governing recrystallization mechanism of high SFE materials. This is the case for Ti and Ni [35]. CDRX is divided into two different recrystallization mechanisms, including geometric dynamic recrystallization (GDRX) and rotational dynamic recrystallization (RDRX). In the GDRX mechanism, refined equiaxed grains are formed by serrations and pinching-off of HAGBs during deformation [10]. GDRX mechanism can be seen at the marked area at Ni/Ni particle boundaries of Fig. 2 (b) with d and Fig. 7, which also has been reported in the literature [36].

RDRX mechanism is considered governing the DRX by a rotational mechanism with the following steps [34, 36]: In the first stages of impact, homogeneous dislocation distribution are generated at sheared zones of single splats (and highly strained interface areas in multiple impacts in a complete coating) [37]. As deformation continues, it stimulates activation of different dislocation sources within the grains, which increases the dislocation density. The generated dislocations annihilate or rearrange themselves as elongated dislocation cells with a dynamic recovery mechanism to minimize the energy. Upon continued deformation, the generated elongated dislocation cell become sub-grains with significant misorientations (elongated grains in Fig. 7). In the last step of DRX, these sub-grains break up into equiaxed grains with a rotational mechanism to minimize interfacial energy (equiaxed grains formed by RDRX in Fig. 7) [2, 34]. Such rotational mechanism of DRX can be seen in Fig. 5, which is marked with c, as reported in the literature [36].

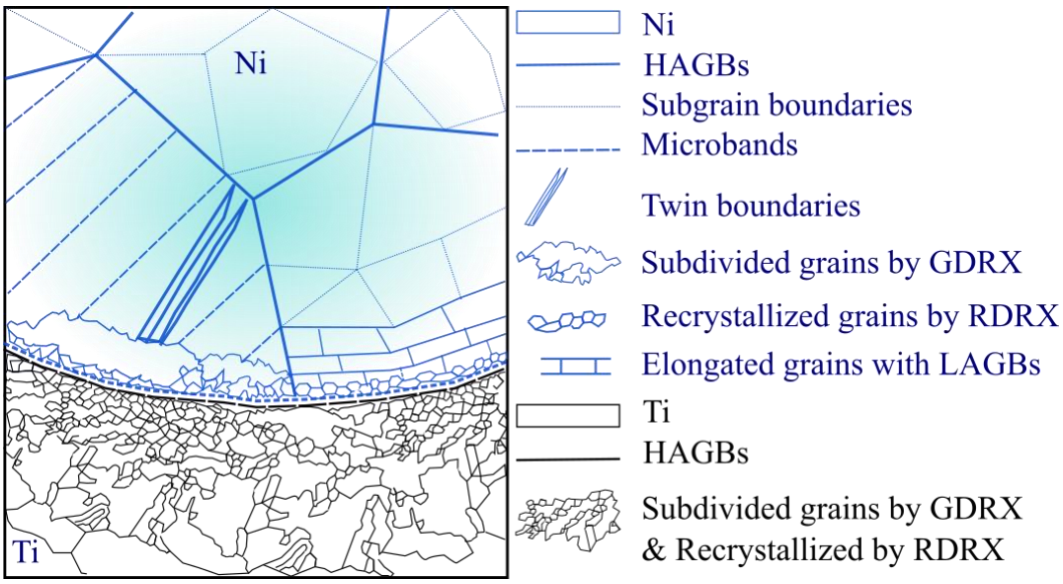

Figure 7. Schematic of the dynamic microstructure evolution of Ni and Ti at cold sprayed composite coating.

Based on experimental observations and FEM modeling results, DRX was mostly observed at the highly strained areas of the splat interface. At the inner boundaries toward the interior of the splats an elongated structure (elongated grains in Fig. 7) can be seen that yet rotated to form HAGBs. As Fig.7 shows, in the interior of the particle far from the interface which deformed at lower stress, strain, strain rate, and temperature, microstructure evolution is limited to dislocation cell formation and different orientations inside the grains.

For Ni splats, twins form at highly strained areas, mostly at splat boundaries, where deformation by twinning is more favorable than dislocation cell formation either as a result of high strain rate and/or preference of twins in the specific orientations. For Ti splat, as reported in the literature, deformation begins by slip. However, because of insufficient slip systems to accommodate the imposed strain, slip is soon accompanied by twinning as an important deformation mode [27]. This different deformation and grain refinement behavior of materials, combined with inherent

heterogeneous deformation of splats in CS, can be employed in a fast and near net shape, consolidating of a wide variety of single component or composite heterogeneous structures.

5. Conclusion

In this study, the microstructure evolution of Ni-Ti composite upon CS deposition was investigated with EBSD analyses, and dynamic heterogeneous structure evolution was explored in composite coating. Findings showed that when the Ni splats are perused from boundaries to the splats' interior, the refined fine grains merge with the twins/micro-bands with a thickness of 500 nm (or less) and LAGBs with some sub-grains formed in interior grains. It was observed that the CDRX-base mechanism controls the refinement process either by GDRX or RDRX. Almost similar microstructure evolution was observed for Ti with the only difference that DRX was more pronounced at all around the Ti splat boundaries with the refined area being extended almost to the center of the splats, which related to differences of materials properties and the effect of dissimilar materials' interaction. Based on the findings, it can be concluded that the inherent heterogeneous deformation of splats in CS combined with different deformation behavior of materials in mixed powders can be used for in situ consolidations of a wide variety of single component or composite heterogeneous structures.

6. References

[1] A.Y. Chen, H.H. Ruan, J. Wang, H.L. Chan, Q. Wang, Q. Li, J. Lu, The influence of strain rate on the microstructure transition of 304 stainless steel, Acta Mater. 59 (2011) 3697-3709, https://doi.org/10.1016/j.actamat.2011.03.005.

[2] Z. Liu, H. Wang, M. Haché, E. Irissou, Y. Zou, Formation of refined grains below 10 nm in size and nanoscale interlocking in the particle–particle interfacial regions of cold sprayed pure aluminum, Scripta Mater. 177 (2020) 96-100, https://doi.org/10.1016/j.scriptamat.2019.09.018.
[3] X. Wu, Y. Zhu, Heterogeneous materials: a new class of materials with unprecedented mechanical properties, Mater. Res. Lett. 5 (2017) 527-532, https://doi.org/10.1080/21663831.2017.1343208.
[4] Y. Zhu, K. Ameyama, P.M. Anderson, I.J. Beyerlein, H. Gao, H.S. Kim, E. Lavernia, S. Mathaudhu, H. Mughrabi, R.O. Ritchie, N. Tsuji, X. Zhang, X. Wu, Heterostructured materials: superior properties from hetero-zone interaction, Mater. Res. Lett. 9 (2021) 1-31, https://doi.org/10.1080/21663831.2017.1343208.
[5] J. Li, Q. Zhang, R. Huang, X. Li, H. Gao, Towards understanding the structure–property relationships of heterogeneous-structured materials, Scripta Mater. 186 (2020) 304-311, https://doi.org/10.1016/j.scriptamat.2020.05.013.
[6] Z. Liu, H. Wang, M.J.R. Haché, X. Chu, E. Irissou, Y. Zou, Prediction of heterogeneous microstructural evolution in cold-sprayed copper coatings using local Zener-Hollomon parameter and strain, Acta Mater. (2020) https://doi.org/10.1016/j.actamat.2020.04.041.
[7] H. Assadi, F. Gärtner, T. Stoltenhoff, H. Kreye, Bonding mechanism in cold gas spraying, Acta Mater. 51 (2003) 4379-4394, https://doi.org/10.1016/S1359-6454(03)00274-X.
[8] A. Papyrin, V. Kosarev, S. Klinkov, A. Alkimov, V. Fomin, Chapter 5 - Current status of the cold spray process, Cold Spray Technology, Elsevier, Oxford, 2007, pp. 248-323, https://doi.org/10.1016/B978-008045155-8/50005-3.
[9] R. McCune, A. Papyrin, J. Hall, W. Riggs, P. Zajchowski, An exploration of the cold gas-dynamic spray method for several materials systems, ASM International, Materials Park, OH (United States), 1995.
[10] T. Liu, J.D. Leazer, L.N. Brewer, Particle deformation and microstructure evolution during cold spray of individual Al-Cu alloy powder particles, Acta Mater. 168 (2019) 13-23, https://doi.org/10.1016/j.actamat.2019.01.054.
[11] X.-T. Luo, C.-X. Li, F.-L. Shang, G.-J. Yang, Y.-Y. Wang, C.-J. Li, High velocity impact induced microstructure evolution during deposition of cold spray coatings: A review, Surf. Coat. Technol. 254 (2014) 11-20, https://doi.org/10.1016/j.surfcoat.2014.06.006.
[12] M.R. Rokni, S.R. Nutt, C.A. Widener, V.K. Champagne, R.H. Hrabe, Review of Relationship Between Particle Deformation, Coating Microstructure, and Properties in High-Pressure Cold Spray, J. Therm. Spray Technol. 26 (2017) 1308-1355, https://doi.org/10.1007/s11666-017-0575-0.
[13] W. Li, K. Yang, D. Zhang, X. Zhou, X. Guo, Interface behavior of particles upon impacting during cold spraying of Cu/Ni/Al mixture, Mater. Des. 95 (2016) 237-246, https://doi.org/10.1016/j.matdes.2016.01.122.
[14] R. Ghelichi, M. Guagliano, Coating by the cold spray process: a state of the art, Frattura ed Integrità Strutturale (2009) 30-44, https://doi.org/10.3221/IGF-ESIS.08.03.
[15] G.T. Gray III, High-strain-rate deformation: mechanical behavior and deformation substructures induced, Annu. Rev. Mater. Res. 42 (2012) 285-303, https://doi.org/10.1146/annurev-matsci-070511-155034.
[16] R. Nikbakht, H. Assadi, B. Jodoin, Intermetallic Phase Evolution of Cold-Sprayed Ni-Ti Composite Coatings: Influence of As-Sprayed Chemical Composition, J. Therm. Spray Technol. (2020) https://doi.org/10.1007/s11666-020-01112-8.

[17] R. Nikbakht, S.H. Seyedein, S. Kheirandish, H. Assadi, B. Jodoin, Asymmetrical bonding in cold spraying of dissimilar materials, Appl. Surf. Sci. 444 (2018) 621-632, https://doi.org/10.1016/j.apsusc.2018.03.103.
[18] R. Nikhbakht, M. Saadati, M. Jahazi, H. Assadi, B. Jodoin, EBSD Analysis Enhancement of Cold Sprayed Composite Materials: Sample Preparation, Annealing, and Scan Optimization, Microscopical Society Symposium of Canada, Université de Sherbrooke, Québec, Canada, 2020.
[19] Z. Arabgol, M. Villa Vidaller, H. Assadi, F. Gärtner, T. Klassen, Influence of thermal properties and temperature of substrate on the quality of cold-sprayed deposits, Acta Mater. 127 (2017) 287-301, https://doi.org/10.1016/j.actamat.2017.01.040.
[20] F. Zhao, L. Wang, D. Fan, B.X. Bie, X.M. Zhou, T. Suo, Y.L. Li, M.W. Chen, C.L. Liu, M.L. Qi, M.H. Zhu, S.N. Luo, Macrodeformation Twins in Single-Crystal Aluminum, Phys. Rev. Lett. 116 (2016) 075501, https://doi.org/10.1103/PhysRevLett.116.075501.
[21] M. Meyers, H. Jarmakani, E. Bringa, B. Remington, Dislocations in shock compression and release, Dislocations in Solids 15 (2009) 91-197, https://doi.org/10.1016/S1572-4859(09)01502-2.
[22] S. Zhao, Z. Li, C. Zhu, W. Yang, Z. Zhang, D.E.J. Armstrong, P.S. Grant, R.O. Ritchie, M.A. Meyers, Amorphization in extreme deformation of the CrMnFeCoNi high-entropy alloy, Sci. Adv 7 (2021) eabb3108, 10.1126/sciadv.abb3108.
[23] P.C. King, S.H. Zahiri, M. Jahedi, Microstructural Refinement within a Cold-Sprayed Copper Particle, Metall. Mater. Trans. A 40 (2009) 2115-2123, https://doi.org/10.1007/s11661-009-9882-5.
[24] Y. Zhang, N. Brodusch, S. Descartes, R.R. Chromik, R. Gauvin, Microstructure refinement of cold-sprayed copper investigated by electron channeling contrast imaging, Microsc. Microanal 20 (2014) 1499-1506.
[25] C. Borchers, F. Gärtner, T. Stoltenhoff, H. Assadi, H. Kreye, Microstructural and macroscopic properties of cold sprayed copper coatings, J. Appl. Phys. 93 (2003) 10064-10070.
[26] G. Bae, K. Kang, C. Lee, Nanoscale deformation twinning at ultrahigh strain rates during kinetic spraying of nickel, Mater. Lett. 89 (2012) 320-323, https://doi.org/10.1016/j.matlet.2012.08.133.
[27] J.Z. Lu, L.J. Wu, G.F. Sun, K.Y. Luo, Y.K. Zhang, J. Cai, C.Y. Cui, X.M. Luo, Microstructural response and grain refinement mechanism of commercially pure titanium subjected to multiple laser shock peening impacts, Acta Mater. 127 (2017) 252-266, https://doi.org/10.1016/j.actamat.2017.01.050.
[28] D. Goldbaum, R.R. Chromik, N. Brodusch, R. Gauvin, Microstructure and mechanical properties of Ti cold-spray splats determined by electron channeling contrast imaging and nanoindentation mapping, Microsc. Microanal 21 (2015) 570-581, https://doi.org/10.1017/S1431927615000240.
[29] G. Chin, W. Hosford, D. Mendorf, Accommodation of constrained deformation in fcc metals by slip and twinning, Proc. Math. Phys. Eng. Sci. 309 (1969) 433-456, https://doi.org/10.1098/rspa.1969.0051.
[30] L.E. Murr, E. Esquivel, Observations of common microstructural issues associated with dynamic deformation phenomena: Twins, microbands, grain size effects, shear bands, and dynamic recrystallization, J Mater Sci 39 (2004) 1153-1168.
[31] J. Qin, Q. Huang, X. Wang, X. Suo, J. Wang, H. Li, Interfacial metal/ceramic bonding mechanism for metallization of ceramics via cold spraying, J. Mater. Process. Technol. 288 (2021) 116845, https://doi.org/10.1016/j.jmatprotec.2020.116845.

[32] A. Rollett, F. Humphreys, G.S. Rohrer, M. Hatherly, Recrystallization and related annealing phenomena, Elsevier2004.
[33] R. Nikbakht, S.H. Seyedein, S. Kheirandish, H. Assadi, B. Jodoin, The role of deposition sequence in cold spraying of dissimilar materials, Surf. Coat. Technol. 367 (2019) 75-85, https://doi.org/10.1016/j.surfcoat.2019.03.065.
[34] M. Meyers, V. Nesterenko, J. LaSalvia, Y. Xu, Q. Xue, Observation and modeling of dynamic recrystallization in high-strain, high-strain rate deformation of metals, J PHYS IV 10 (2000) Pr9-51-Pr9-56, https://doi.org/10.1051/jp4:2000909
[35] K. Huang, R.E. Logé, A review of dynamic recrystallization phenomena in metallic materials, Mater. Des. 111 (2016) 548-574, https://doi.org/10.1016/j.matdes.2016.09.012.
[36] Y. Zou, W. Qin, E. Irissou, J.-G. Legoux, S. Yue, J.A. Szpunar, Dynamic recrystallization in the particle/particle interfacial region of cold-sprayed nickel coating: Electron backscatter diffraction characterization, Scripta Mater. 61 (2009) 899-902, https://doi.org/10.1016/j.scriptamat.2009.07.020.
[37] S. Rahmati, R.G.A. Veiga, B. Jodoin, A. Zúñiga, Crystal orientation and grain boundary effects on plastic deformation of FCC particles under high velocity impacts, Materialia 15 (2021) 101004, https://doi.org/10.1016/j.mtla.2021.101004.